Journal of the Mechanical Behavior of Biomedical Materials 88 (2018) 29–40

Contents lists available at ScienceDirect

Journal of the Mechanical Behavior of Biomedical Materials

journal homepage: www.elsevier.com/locate/jmbbm

A new model of passive muscle tissue integrating Collagen Fibers: Consequences for muscle behavior analysis

Ali-Akbar Karkhaneh Yousefi[a,*], Mohammad Ali Nazari[a], Pascal Perrier[b], Masoud Shariat Panahi[a], Yohan Payan[c]

[a] School of Mechanical Engineering, College of Engineering, University of Tehran, Tehran, Iran
[b] Univ. Grenoble Alpes, CNRS, Grenoble INP, Gipsa-lab, F38000 Grenoble, France
[c] Univ. Grenoble Alpes, CNRS, Grenoble INP, TIMC-IMAG, F38000 Grenoble, France

ARTICLE INFO

Keywords:
Muscle model
Passive behavior
Collagen Fibers
Inverse FEA

ABSTRACT

Mechanical properties of muscle tissue are crucial in biomechanical modeling of the human body. Muscle tissue is a combination of Muscle Fibers (MFs) and connective tissue including collagen and elastin fibers. There are a lot of passive muscle models in the literature but most of them do not consider any distinction between Collagen Fibers (CFs) and MFs, or at least do not consider the mechanical effects of the CFs on the Three-Dimensional (3-D) behavior of tissue. As a consequence, unfortunately, they cannot describe the observed stress-stretch behavior in tissue in which the reinforced direction is not parallel to the MF direction. In this research, a new passive muscle model is presented, in which the CFs are separately considered in the formulation: they are distributed along the MFs in a cross-shaped arrangement. Thanks to this new architecture, a mechanical reinforced direction can be proposed, in addition to the muscle main fiber direction.

The passive biomechanical properties of the genioglossus muscle of a bovine tongue have been measured under uniaxial tensile tests. To characterize the 3-D response of the tissue, tests have been performed in different directions with respect to the MF direction. Moreover, a Constitutive Law (CL) has been proposed for modeling this behavior. In addition to our measurements on the bovine genioglossus muscle, results published in the literature on experimental data from the longissimus dorsi of pigs and the chicken pectoralis muscle were used to appraise the applicability of the proposed model. It is demonstrated that the proposed passive muscle model provides an accurate description of the fiber-oriented nature of muscle tissue. Also, it has been shown that using Finite Element Analysis (FEA) it might be possible to predict the angle θ between CFs and MF.

1. Introduction

Accounting properly the physical characteristics of the musculoskeletal system significantly affects the accuracy of computational models in predicting human body behavior in a variety of applications such as impact biomechanics, surgical simulations and tissue engineering (Takaza et al., 2013). Besides an accurate geometrical description, these models also need a comprehensive Constitutive Law (CL) to fully take into consideration the tissue material properties such as nonlinearity, viscoelasticity and anisotropy (Yousefi et al., 2018; Van Loocke et al., 2006; Gras et al., 2012; Morrow et al., 2010; Parente et al., 2009; Calvo et al., 2010; Pioletti et al., 1998). In most of the studies, skeletal muscles have been considered as fiber-reinforced materials in which the stiffest direction is parallel to the Muscle Fiber (MF) direction (Morrow et al., 2010; Calvo et al., 2010; Martins et al., 1998; Humphrey and Yin, 1987; Parente et al., 2009; Song et al., 2007; Blemker et al., 2005). However, to the authors' knowledge, muscles have not been sufficiently investigated experimentally yet and the available CLs fail in describing their Three-Dimensional (3-D) passive behavior, especially for those that show less resistance in loading along the MF direction (Gindre et al., 2013; Nie et al., 2011; Wheatley et al., 2016). Takaza et al. (2013) measured passive stress-stretch responses of the pig longissimus dorsi muscle under uniaxial tensile tests. The reported results show that the MF direction is the weakest direction in this muscle in terms of mechanical resistance to elongation. A more surprising behavior has been reported for the chicken pectoralis muscle in which the tissue is stiffer in the direction of 45° with respect to the MF direction (Mohammadkhah et al., 2016).

Muscle tissue has frequently been considered as a network of MFs, Collagen Fibers (CFs), and elastin fibers embedded in an isotropic

* Corresponding author.
E-mail address: Ali.karkhaneh@ut.ac.ir (A.-A.K. Yousefi).

https://doi.org/10.1016/j.jmbbm.2018.07.042
Received 24 May 2018; Received in revised form 26 July 2018; Accepted 30 July 2018
Available online 01 August 2018
1751-6161/

matrix (Hernández et al., 2011). The MFs are surrounded by connective tissue of three different anatomical properties made of CFs, which are from the most external to the most internal level: epimysium (surrounding the whole muscle), perimysium (surrounding fiber bundles), and endomysium (around each individual fiber) (Purslow, 2010). The main course of the CFs determines one of the directions of material anisotropy and such fibers are mainly responsible for the passive behavior of the tissue. The active response, which is responsible for the contractile behavior, usually refers to the response of the muscular fibers (Grasa et al., 2016; Gindre et al., 2013).

In some long strap-like muscles, two parallel sets of wavy CFs in a crossed-ply arrangement have been observed in the epimysium (Purslow, 1989, 2010). Depending on the sarcomere length, the mean CF angle with respect to the MF axis varies in the range of 20–80°. This explains why mechanical passive properties of some muscles are stronger in the direction transverse to the MF direction (Takaza et al., 2013; Mohammadkhah et al., 2016; Wheatley et al., 2016). For these muscles, the available CLs, in which the CFs and the MFs are identified with the same direction, cannot describe the observed stress-stretch behavior. In these models, the existence of any reinforced direction other than the MF direction may impose some negative values on the anisotropic part of the stress tensor, which violates the convexity condition of the Strain Energy Function (SEF). To the authors knowledge, only for the cases in which the stiffest direction is perpendicular to the MF direction, the convexity condition is satisfied and it is possible to explain this behavior either using the invariants and structural tensors proposed by Schröder and Neff (2003) or assuming an ellipsoidal distribution of fibers in muscles in which the shortest diameter is along the direction of MFs (Wheatley et al., 2017). So, it seems that the effects of the MF and CFs and their respective directions have to be separately defined in the passive CLs of muscle tissue.

The tongue is one of the most intriguing human organs because it plays a vital role in respiration, suckling, gathering and manipulating food, swallowing, and speech. The mammalian tongue is a complex muscular structure, which is composed of the mucous membrane, intrinsic and extrinsic muscles, and connective tissue (Shall, 2012). Extrinsic muscles originate from bones external to the tongue and insert into the body of the tongue: the genioglossus, the hyoglossus, the styloglossus and the palatoglossus. These muscles are the main responsible for the large displacements and shaping of the tongue. Intrinsic muscles are fully embedded in the body of the tongue and determine more locally the shape of the tongue: the superior longitudinal, the inferior longitudinal, the verticalis and the transversalis (Gérard et al., 2006). Each of these muscles has some specific orientation dependent properties.

The human tongue has been widely investigated experimentally and numerically to describe its actions in the vocal tract (Rohan et al., 2017;, Gérard et al., 2005, 2006; Dang and Honda, 2002; Vogt et al., 2006; Fujita et al., 2007). Yousefi et al. (2018) proposed a visco-hyperelastic CL to describe the rate-dependent and anisotropic stress-stretch behavior in the superior longitudinal muscle and the mucous membrane of bovines. Finite element models intend to improve the understanding of the role of the tongue in speech production (Buchaillard et al., 2009) and swallowing (Stavness et al., 2006). Unfortunately, the complex behavior of the tongue tissue has been reduced by simplified models in previous researches. Due to the lack of experiments in tongue tissue, a passive CL considering specifically the nonlinear nature and the anisotropic behavior of each muscle has not been proposed yet.

In higher order mammals, the musculatures of tongues are similar (Gilbert et al., 2006; Shall, 2012). It was therefore decided to focus this paper on bovine tongue tissue since it is still complicated to characterize the biomechanical properties of human tongue tissue. It is hypothesized that tongue tissue has similar passive constitutive behavior in humans and bovines. Obviously, the bovine tongue, which wraps around the grass and heaves to rip it off, has very specific abilities. We believe that this peculiarity can be explained by the size of the bovine tongue and by its capacity of producing an active force that is significantly higher than human tongue (Yousefi et al., 2018).

In this research, the mechanical properties of the genioglossus muscle of bovine tongue are investigated to propose a new passive mechanical model for muscle tissue, which can completely predict its fiber-oriented responses. To do this, the stress-stretch response of the bovine genioglossus muscle is measured under uniaxial tensile tests. Furthermore, a new CL is proposed for the passive behavior of muscle tissue which can specifically take into consideration the 3-D effects of the CFs. To evaluate the proposed model, its accuracy in approximating the experimental data is demonstrated for our data about the bovine genioglossus tissue as well as for published experimental data about the pig longissimus dorsi muscle (Takaza et al., 2013) and the chicken pectoralis muscle (Mohammadkhah et al., 2016).

The paper is organized in the following manner. In Section 2, a new model of passive muscle behavior describing the nonlinear and orientation dependent response of muscle tissue is proposed. In Section 3, the details of the bovine tongue sample preparation and test procedures are presented. In addition, the proposed model is used to approximate the stress-stretch response of the bovine tongue genioglossus muscle. The ability of this model in predicting the experimental data on the pig longissimus dorsi muscle and the chicken pectoralis muscle is examined in Section 4. A discussion with perspectives closes this article.

2. A new passive muscle model

Most of the passive muscle models in the literature do not consider any distinction between CFs and MFs, or at least do not consider the mechanical effects of CFs on the 3-D behavior of tissue. These models cannot provide a realistic account of the observed stress-stretch responses in muscle tissue, especially in tissue that amazingly shows stronger resistance against elongation in a direction different from the MF alignment (Takaza et al., 2013; Hernández et al., 2011; Mohammadkhah et al., 2016; Wheatley et al., 2016). Recently, Grasa et al. (2016) have introduced the CFs in their passive muscle model that can describe such an amazing stress-stretch behavior, but this model does not include the 3-D distribution of the CFs. Moreover, Wheatley et al. (2017) have proposed a model for muscles in which it is possible to predict that the stiffest direction can be perpendicular to the MFs direction. But their model uses a lot of material parameters and cannot explain the cases in which the stiffest direction is neither parallel to the MFs direction nor perpendicular to it (Mohammadkhah et al., 2016). From our point of view, to model the passive behavior of muscle tissue, it is essential to separately take into consideration the direction and action of the CFs, which are distinct from the ones of the MFs.

2.1. Structure of the muscle tissue

Regarding the approximately helical distribution of the CFs along each MF (Purslow, 2010; Gindre et al., 2013), we propose to consider them as a pair of crossed fibers in any plane containing the MFs as they can be approximately observed in practice in any cross-section parallel to the MF direction (Purslow, 1989). Fig. 1 schematically shows a slice of a muscle tissue and two arbitrary perpendicular planes P1 and P2. These planes are mechanically equivalent and contain the cross-shaped arrangement of CFs with angle θ with respect to the MF direction. Regardless of the dispersion of CFs, angle θ represents the average direction of CFs in skeletal muscles. As depicted in Fig. 1, due to the symmetrical distribution of the CFs along the MFs, our model of the passive muscle tissue is similar to the transversely isotropic materials which show the same material properties in any direction in the isotropy plane which is perpendicular to the MF direction. But for $\theta \neq 0^{\circ}$, compared with the transversely isotropic materials, the reinforced direction is not necessarily either in the isotropy plane or the normal vector of the isotropy plane, namely the MF direction. Thus, the

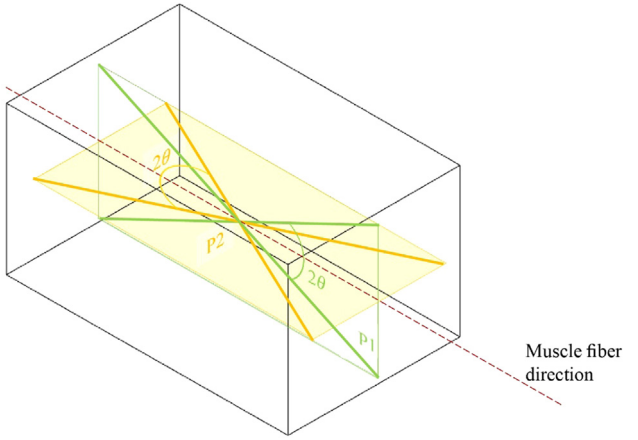

Fig. 1. Schematic model of a muscle tissue in which a pair of cross-shaped CFs exists in any plane containing the MF direction.

proposed model in Fig. 1 provides the possibility of the existence of some other direction with mechanical properties stronger than the ones in the direction of MFs.

Another significant effect of the CFs on the stress-stretch response, which has not been considered in the literature yet, is their 3-D nature as they are distributed in any plane containing the MFs. To characterize this, let us suppose that a muscle sample undergoes a uniaxial extension along the direction $X1$ with acute angle ϕ with respect to the direction of the MFs, as depicted in Fig. 2. In general, there is a coordinate system $X1X2X3$ which at least includes one of the symmetry planes of this sample. Such a plane contains $X1$ and the MF direction as the CFs symmetrically surround it. Hence, there is no shear deformation out of this plane. Further, let $X2$ be in the plane of symmetry and $X3$ perpendicular to this plane.

In Fig. 2, as mentioned before, there are two mechanically equivalent CFs with unit vectors $\mathbf{a}_1 = (\cos(\theta - \phi), \sin(\theta - \phi), 0)$ and $\mathbf{a}_2 = (\cos(\theta + \phi), -\sin(\theta + \phi), 0)$ in the plane $X1X2$. To measure the contribution of the other pairs of CFs to the stress response out of the $X1X2$ plane, it is sufficient to consider the one which is located in the plane constructed with $X3$ and the MF direction. Furthermore, it can easily be shown that these two families of CFs are along the unit vectors $\mathbf{g}_1 = (\cos\theta\cos\phi, -\cos\theta\sin\phi, \sin\theta)$ and $\mathbf{g}_2 = (\cos\theta\cos\phi, -\cos\theta\sin\phi, -\sin\theta)$.

2.2. Kinematics and stress tensors

A CL has to be chosen to describe the stress-stretch relationship of

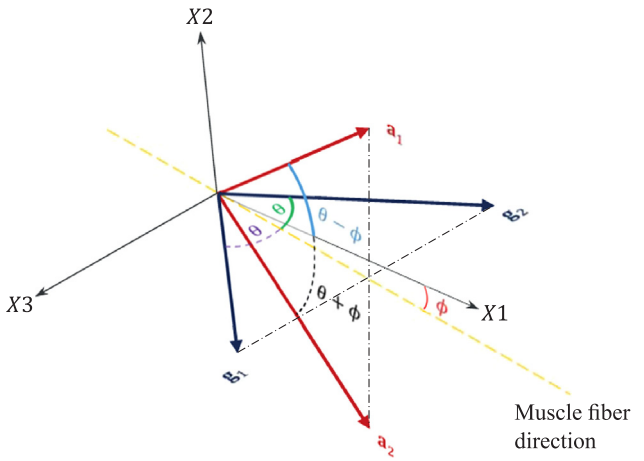

Fig. 2. The configuration of the CFs and the MF direction in the coordinate system *X1X2X3*.

passive muscle tissue. Chagnon et al. (2015) reviewed and classified the most popular hyperelastic CLs for soft tissue. For a specific muscle tissue, based upon the material structure and shape of the measured stress-stretch curves, an appropriate CL can be defined. To show how a stress-stretch response is related to a CL, let us briefly review the large deformation formulation in the framework of hyperelasticity. Let $\mathbf{X}$ and $\mathbf{x}$ be the position vector of material points in the reference (undeformed) and deformed configurations, respectively. For any function χ describing the motion $\mathbf{x} = \chi(\mathbf{X})$ which maps any position vector of the reference configuration to the deformed configuration, let $\mathbf{F}(\mathbf{X}) = \partial\mathbf{x}/\partial\mathbf{X}$ be the deformation gradient tensor and $J = \det\mathbf{F}(\mathbf{X}) > 0$ the Jacobian representing the ratio of volume change during the deformation. Following Flory (1961), $\mathbf{F}$ can be decomposed as:

$$\mathbf{F} = (J^{1/3}\mathbf{I})\bar{\mathbf{F}} \tag{1}$$

with a dilatational part $J^{1/3}\mathbf{I}$ and a distortional part $\bar{\mathbf{F}}$, in which $\mathbf{I}$ represents the second order identity tensor. The modified right Cauchy-Green strain tensor is given by $\bar{\mathbf{C}} = \bar{\mathbf{F}}^{\mathrm{T}}\bar{\mathbf{F}}$. For 3-D hyperelastic CLs representing isotropic materials, the invariants of a strain tensor are used as variables to define a SEF in order to meet the requirement of objectivity. So, taking $\bar{\mathbf{C}}$ as this strain tensor, its two modified principal invariants are defined as:

$$\bar{I}_1 = \mathrm{tr}\bar{\mathbf{C}}, \quad \bar{I}_2 = \frac{1}{2}[(\mathrm{tr}\bar{\mathbf{C}})^2 - \mathrm{tr}(\bar{\mathbf{C}}^2)] \tag{2}$$

For anisotropic materials reinforced with two families of fibers, the modified principal invariants defined by Eq. (2) are not sufficient to describe the behavior. Hence, for such materials with two preferred fiber directions specified by the referential unit vectors $\mathbf{n}_1$ and $\mathbf{n}_2$, the symmetric structural tensors $\mathbf{A}_1$ and $\mathbf{A}_2$ are defined as:

$$\mathbf{A}_1 = \mathbf{n}_1 \otimes \mathbf{n}_1, \quad \mathbf{A}_2 = \mathbf{n}_2 \otimes \mathbf{n}_2 \tag{3a}$$

$$\bar{I}_{4\mathbf{a}_1} = \mathrm{tr}(\bar{\mathbf{C}}\mathbf{A}_1) \tag{3b}$$

$$\bar{I}_{4\mathbf{a}_2} = \mathrm{tr}(\bar{\mathbf{C}}\mathbf{A}_2) \tag{3c}$$

in which $\bar{I}_{4\mathbf{a}_1}$ and $\bar{I}_{4\mathbf{a}_2}$ are modified additional invariants (pseudo-invariants), which are the most common variables in defining the CLs for anisotropic materials (Spencer, 1984). Also, $\otimes$ in Eq. (3a) represents the dyadic multiplication of two vectors.

In hyperelasticity, to describe the stress response for muscle tissue, it is postulated that a scalar-valued free energy function exists, which is called the Helmholtz free energy function ψ, also referred to as strain energy function or elastic potential energy function (Gasser et al., 2006). For isothermal processes, the thermodynamical principles reduce to the satisfaction of the Clausius-Duhem inequality

$$\left(\mathbf{S} - 2\frac{\partial\psi}{\partial\mathbf{C}}\right) : \frac{\dot{\mathbf{C}}}{2} \geq 0 \quad \forall\mathbf{C}, \dot{\mathbf{C}} \tag{4}$$

where the operator ":" represents the double contraction of two tensors, $\mathbf{C} = J^{2/3}\bar{\mathbf{C}}$ represents the right Cauchy-Green strain tensor, $\dot{\mathbf{C}}$ is its material time derivative, and $\mathbf{S}$ is the second Piola-Kirchhoff stress tensor. Without energy dissipations, $\mathbf{S} = 2\frac{\partial\psi}{\partial\mathbf{C}}$ can be a solution for Eq. (4).

2.3. Constitutive law

To describe the stress-stretch response of the muscle tissue which is assumed to behave nearly incompressible, it was decided to propose the SEF ψ in the decoupled form with a purely volumetric part ψ_{vol} as a measure of the required strain energy to change the volume and a purely isochoric part ψ_{iso} representing the stored strain energy by the distortion part of a deformation. The volumetric part is a function of J and the isochoric part is defined as a function of the modified right Cauchy-Green strain tensor, the structural tensors constructed by the direction of the CFs and MFs, and the activation parameter α which

determines the amount of the active stress in the muscle tissue. Therefore, in the general form, the SEF of the skeletal muscles can be stated as:

$$\psi(\mathbf{C}, \mathbf{A}_1, \mathbf{A}_2, \mathbf{G}_1, \mathbf{G}_2, \mathbf{A}_{mf}, \alpha) = \psi_{vol}(J) + \psi_{iso}(\bar{\mathbf{C}}, \mathbf{A}_1, \mathbf{A}_2, \mathbf{G}_1, \mathbf{G}_2, \mathbf{A}_{mf}, \alpha) \tag{5}$$

with the structural tensors $\mathbf{A}_1 = \mathbf{a}_1 \otimes \mathbf{a}_1$, $\mathbf{A}_2 = \mathbf{a}_2 \otimes \mathbf{a}_2$, $\mathbf{G}_1 = \mathbf{g}_1 \otimes \mathbf{g}_1$, and $\mathbf{G}_2 = \mathbf{g}_2 \otimes \mathbf{g}_2$ in which the unit vectors $\mathbf{a}_1$, $\mathbf{a}_2$, $\mathbf{g}_1$, and $\mathbf{g}_2$ have been introduced in Fig. 2. Also, $\mathbf{A}_{mf} = \mathbf{a}_{mf} \otimes \mathbf{a}_{mf}$ with the referential unit vector $\mathbf{a}_{mf}$ in the direction of the MFs. Eq. (5) shows how the proposed model of this study distinguishes between the CFs and the MFs. In other words, $\mathbf{A}_{mf}$ is required to define to active response.

Moreover, the isochoric part of the SEF itself can be divided into the passive (ψ_p) and active (ψ_a) parts as:

$$\psi_{iso}(\bar{\mathbf{C}}, \mathbf{A}_1, \mathbf{A}_2, \mathbf{G}_1, \mathbf{G}_2, \mathbf{A}_{mf}, \alpha) = \psi_p(\bar{\mathbf{C}}, \mathbf{A}_1, \mathbf{A}_2, \mathbf{G}_1, \mathbf{G}_2) + \psi_a(\bar{\mathbf{C}}, \mathbf{A}_{mf}, \alpha) \tag{6}$$

Since characterizing the passive behavior of the muscle tissue is the concern of this study, from now on the active part of the SEF is discarded. ψ_{iso} is generally defined by the invariants $\bar{I}_1$, $\bar{I}_2$, J, and $\bar{I}_4$. Hence, the SEF is proposed as:

$$\psi(\bar{I}_1, \bar{I}_2, J, \bar{I}_4) = \psi_{vol}(J) + \psi_{iso}(\bar{I}_1, \bar{I}_2, \bar{I}_4) \tag{7a}$$

$$\psi_{vol}(J) = \frac{1}{2}k(J-1)^2 \tag{7b}$$

$$\psi_{iso}(\bar{I}_1, \bar{I}_2, \bar{I}_4) = c_1(\bar{I}_1-3)^2 + c_2(\bar{I}_2-3) + \frac{c_3}{c_4}\left\{\left(\sqrt{\bar{I}_{4\mathbf{a}_1}}-1\right)^{c_4} + \left(\sqrt{\bar{I}_{4\mathbf{a}_2}}-1\right)^{c_4} + \left(\sqrt{\bar{I}_{4\mathbf{g}_1}}-1\right)^{c_4} + \left(\sqrt{\bar{I}_{4\mathbf{g}_2}}-1\right)^{c_4}\right\} \tag{7c}$$

with the Lagrange multiplier k and the material parameters c_{1-4}. All of the material parameters have to be non-negative to warrant the convexity condition of the SEF. Also, the modified fourth invariants $\bar{I}_{4\mathbf{a}_i}$ and $\bar{I}_{4\mathbf{g}_i}$ are equivalent to the square of the stretch along the unit vectors $\mathbf{a}_i$ and $\mathbf{g}_i$ scaled by $J^{-2/3}$, respectively. These invariants are separately considered in the proposed model to apply the 3-D effects of the CFs on the stress tensor. In Eq. (7c), the first two terms are added to take into account the contribution of the matrix-fiber ensemble in an anisotropic material, and the third term characterizes the CFs resistance to elongation. Since all of the CFs have made of the same matter, they have the same mechanical properties and as a consequence, their contribution has been proposed by the same material parameters in Eq. (7c).

Although recent studies indicate that MFs and CFs have a contribution in compression (Van Loocke et al., 2006, 2008; Böl et al., 2014, 2016), the overall resistance of muscle tissue in compression is a way lower than its resistance against tension (Mohammadkhah et al., 2016). Therefore, since the concern of this study is to approximate the stress-stretch response of muscle tissue in tension, the influence of the resistance of the CFs in compression was considered to be negligible. In other words, for $\bar{I}_{4\mathbf{a}_i}<1$ and $\bar{I}_{4\mathbf{g}_i}<1$, the corresponding anisotropic terms in Eq. (7c) are considered to be negligible.

For the proposed model in Eqs. (7a)–(7c), $\mathbf{S}$ can be defined in the decoupled form too (Holzapfel, 2000). In this manner, $\mathbf{S}$ is given by:

$$\mathbf{S} = 2\frac{\partial \psi}{\partial \mathbf{C}} = \mathbf{S}_{vol} + \mathbf{S}_{iso} \tag{8a}$$

$$\mathbf{S}_{vol} = kJ(J-1)\mathbf{C}^{-1} \tag{8b}$$

$$\mathbf{S}_{iso} = J^{-2/3}\left(\bar{\mathbf{S}} - \frac{1}{3}\mathrm{tr}(\bar{\mathbf{S}}\mathbf{C})\mathbf{C}^{-1}\right) \tag{8c}$$

$$\bar{\mathbf{S}} = 2\frac{\partial \psi_{iso}}{\partial \bar{\mathbf{C}}} = 4c_1(\bar{I}_1-3)\mathbf{I} + 2c_2(\bar{I}_1\mathbf{I} - \bar{\mathbf{C}}) + c_3\left\{\frac{\left(\sqrt{\bar{I}_{4\mathbf{a}_1}}-1\right)^{(c_4-1)}}{\sqrt{\bar{I}_{4\mathbf{a}_1}}}\mathbf{A}_1 + \frac{\left(\sqrt{\bar{I}_{4\mathbf{a}_2}}-1\right)^{(c_4-1)}}{\sqrt{\bar{I}_{4\mathbf{a}_2}}}\mathbf{A}_2 + \frac{\left(\sqrt{\bar{I}_{4\mathbf{g}_1}}-1\right)^{(c_4-1)}}{\sqrt{\bar{I}_{4\mathbf{g}_1}}}\mathbf{G}_1 + \frac{\left(\sqrt{\bar{I}_{4\mathbf{g}_2}}-1\right)^{(c_4-1)}}{\sqrt{\bar{I}_{4\mathbf{g}_2}}}\mathbf{G}_2\right\} \tag{8d}$$

where $\bar{\mathbf{S}}$ is called the fictitious second Piola-Kirchhoff stress tensor. See Holzapfel (2000) for calculating the required derivatives in writing Eqs. (8a)–(8d) and more detailed explanations of extracting Eq. (8c).

Generally, when a muscle tissue is loaded along the $X1$ direction as depicted in Fig. 2, $\mathbf{F}$ can be written as:

$$\mathbf{F} = \begin{bmatrix} F_{11} & F_{12} & 0 \\ F_{21} & F_{22} & 0 \\ 0 & 0 & F_{33} \end{bmatrix} \tag{9}$$

in which the off-diagonal components vanish only for $\phi = 0^\circ$ and $\phi = 90^\circ$; $F_{33} = 1/(F_{11}F_{22}-F_{12}F_{21})$ due to the near incompressibility assumption. Thus, using the relationship $\mathbf{P} = \mathbf{FS}$, from Eqs. (8a)–(8d) and (9), the components of the nominal stress tensor $\mathbf{P}$ can be obtained as a function of the components of $\mathbf{F}$. In general, it is not possible to determine all the components of $\mathbf{F}$ for an arbitrary ϕ. For $\phi \neq 0^\circ$ sample undergoes shear stress in the $X1X2$ plane and for $\phi = 90^\circ$ equality of F_{22} and F_{33} depends on the value of θ. Therefore, there is no explicit relationship between the stress and the controllable parameters of the machine. Thus, an inverse finite element method has to be used in order to determine the uncontrollable components of $\mathbf{F}$ from the experimental data.

2.4. Adjustment of material parameters

The material parameters can be determined by adjusting the nominal stress-stretch relationship in order to fit the experimental data points at $\phi = 0^\circ$ and $\phi = 90^\circ$. Since $\mathbf{P}$ in the case of $\phi = 90^\circ$ is not necessarily only a function of the controllable parameters of the machine, some complementary tools like an Finite Element Analysis (FEA) have to be employed to determine the uncontrollable components of $\mathbf{F}$. To do this, a first guess of the values of the material parameters is inferred from the results of tensile tests at $\phi = 0^\circ$ and $\phi = 90^\circ$ with a MATLAB script based on the Genetic optimization algorithm (Goldberg, 2006), in which $\mathbf{F}$ is assumed to be symmetric in the directions $X2$ and $X3$, which enables to simplify the stress-stretch relationship to a function of stretch F_{11}. In other words, the material parameters are estimated by minimizing the objective function $f(c_i)$ which represents a measure of the error between the experimental stress and the model prediction as:

$$f(c_i) = \frac{1}{m}\sum_{i=1}^{m}\left(P^i_{11exp} - P^i_{11pre}\right)^2_{\phi=0^\circ} + \frac{1}{n}\sum_{j=1}^{n}\left(P^j_{11exp} - P^j_{11pre}\right)^2_{\phi=90^\circ} \tag{10}$$

in which P_{11exp} and P_{11pre} are the experimental and predicted nominal stress values along the direction $X1$, respectively. Also, m and n are the number of data points for the cases of $\phi = 0^\circ$ and 90°.

Then, the tensile test with $\phi = 90^\circ$ is simulated with ABAQUS explicit solver by implementing a user-defined material model in subroutine VUMAT. After the FEA, changes of the non-zero components of $\mathbf{F}$ during the loading time are ready to be used in $\mathbf{P}$. Thus, updated values of the material parameters can be calculated through the optimization process using Eq. (10), in which $\mathbf{F}$ is taken from the FEA. The proposed procedure of the material parameters estimation has to be iterated with the updated parameters to converge to constant values. Fig. 3 shows the required steps to calculate the material parameters c_i of our proposed CL via uniaxial tensile tests.

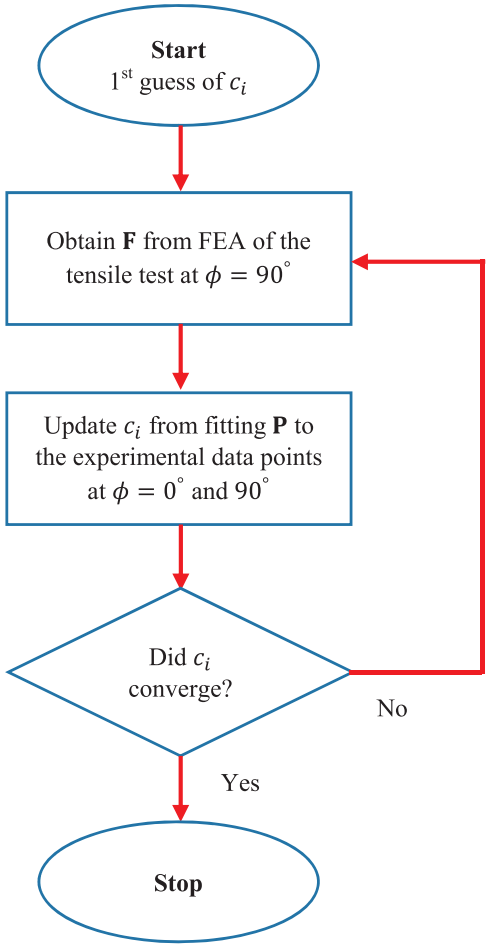

Fig. 3. Flowchart of the material parameters estimation procedure for muscle tissue via uniaxial tensile tests.

3. Bovine tongue genioglossus muscle

In this section, the mechanical properties of the genioglossus muscle of bovine tongue are investigated under uniaxial tensile tests. Furthermore, the proposed CL in Eqs. (7a)–(7c) is evaluated by approximating the measured stress-stretch responses of this muscle.

3.1. Experimental tensile tests

In order to accurately measure the mechanical properties of the bovine tongue tissue, three freshly slaughtered adult bovine tongues were used. Immediately after the sacrifice done early morning, the tongue was cut from the larynx and immersed in a saline solution at 4 °C to keep it fresh and to prevent it from degradation (Hernández et al., 2011; Gras et al., 2012). Due to the complex structure and the direction variation of tongue fibers (Gilbert et al., 2006), cutting an appropriate sample with a fixed fiber direction from each muscle part is difficult in practice. So in the current research, the samples were cut from the genioglossus tissue which is the largest muscle of the tongue. The ratio of the grip-to-grip length to width of the samples was set at least around 7 which was recommended by Hernández-Gascón et al. (2014). Besides, finite element results show that such long ratio is sufficient to achieve a uniform stretch distribution in the central area of a sample even in the presence of the anisotropy and shear deformations. These samples underwent a uniaxial tensile test on a Santam STM-1 machine with a 6 kg full-scale load cell. All of the reported data in this paper have been averaged among the measured stress-stretch behavior in different samples dissected from three bovine tongues. Fig. 4 shows the bovine tongue and a corresponding sample during a tensile test.

The genioglossus originates on the genial tubercle on the inside of the anterior mandible and inserts on the ventromedial base of the tongue. It can therefore pull the tongue toward the mandible and as a result of tissue incompressibility protrude the tongue outside the mouth (Gérard et al., 2006). We assume that the response of the genioglossus tissue to the uniaxial tensile tests is strongly dependent on the angle between the CFs direction and the tensile force. To examine this dependency, some rectangular shape samples were dissected from the genioglossus with angles 90°, 45°, and 0° with respect to the MF alignment. Six samples along the MF direction, five samples at 45°, and five samples at 90° were prepared to measure the average response in the genioglossus tissue. Although there are some difficulties in dissecting samples from muscle tissue, it was tried to cut them in a rectangular shape as much as possible since geometrical imperfections may adversely affect the accuracy of the identified material parameters (Böl et al., 2012). Also, tests were performed at the speed of 2 mm/min to measure only the quasi-static response of the tissue. Table 1 presents the number of samples dissected from the bovine genioglossus muscle and their mean geometrical dimensions as well as the standard deviation values (sdv).

Also, the stretch ratio has been measured by dividing the instantaneous distance between the grips to the initial one. Of course there are some optical techniques to measure the stretch ratio in the central part of a sample, but the differences between these two methods remain less than 1% even after applying 50% of stretch (Tian et al., 2015). After fastening the grips, the amount of the gripped length between the platens was controlled by a marker line on the platens as an indicator to show whether slippage occurred or not. Then, tests started and continued until rupture and the stress-stretch curves have been reported up until a considerable decrease in the load cell. To prevent the damage caused by fastening the grips and increase the friction between the muscle and platens, a particular glue named Mitreapel was used just in those areas. This method considerably facilitates obtaining smoother stress-stretch curves to higher ranges of stretch.

3.2. Model predictions

Experimental tests from samples of the genioglossus muscle have been performed at $\phi = 0^\circ$, 45°, and 90°. Although the angle θ between CFs and MFs has not been experimentally measured, it seems to be possible to estimate this angle thanks to FEA, since θ is a parameter of this analysis. To do this, the material parameters have been determined for different values of θ; then the accuracy of the prediction of each set of θ has been examined. As the genioglossus tissue is stronger when it is loaded perpendicular to the MFs direction, the searching space of angle θ has been limited to values greater than 45°. Following the material parameters estimation procedure described in Fig. 3, c_{1-4} have been accurately determined for some arbitrary values of $\theta = 60^\circ$, 63°, 65°, and 70°. For instance, in the case of $\theta = 65^\circ$, Fig. 5 shows the nominal stress-stretch responses of the proposed model in Eqs. (7a)–(7c) fitted to the experimental data points at $\phi = 0^\circ$ and 90°. The standard deviation curves around the mean values are also shown in gray lines. In this figure, the coefficient of determination R^2, provides a measure of goodness of fitting, shows that the material parameters are well-defined to fit the experimental points. The corresponding estimated values of c_{1-4} and k are provided in Table 2. Also, in Table 2 the goodness of fitting of the proposed model for each set of θ has been provided. The large value of k ensures the incompressibility of material. Moreover, a convergence study to show that the final values of the material parameters are independent of a first guess has been presented in appendix A.

For the cases of $\theta > 63^\circ$, when the genioglossus muscle is extended parallel to the MFs direction, the CFs have no contribution to bearing the tensile load. Although the angle θ has changed, the parameters c_1 and c_2 remained constant in Table 2. It can be explained by the fact that

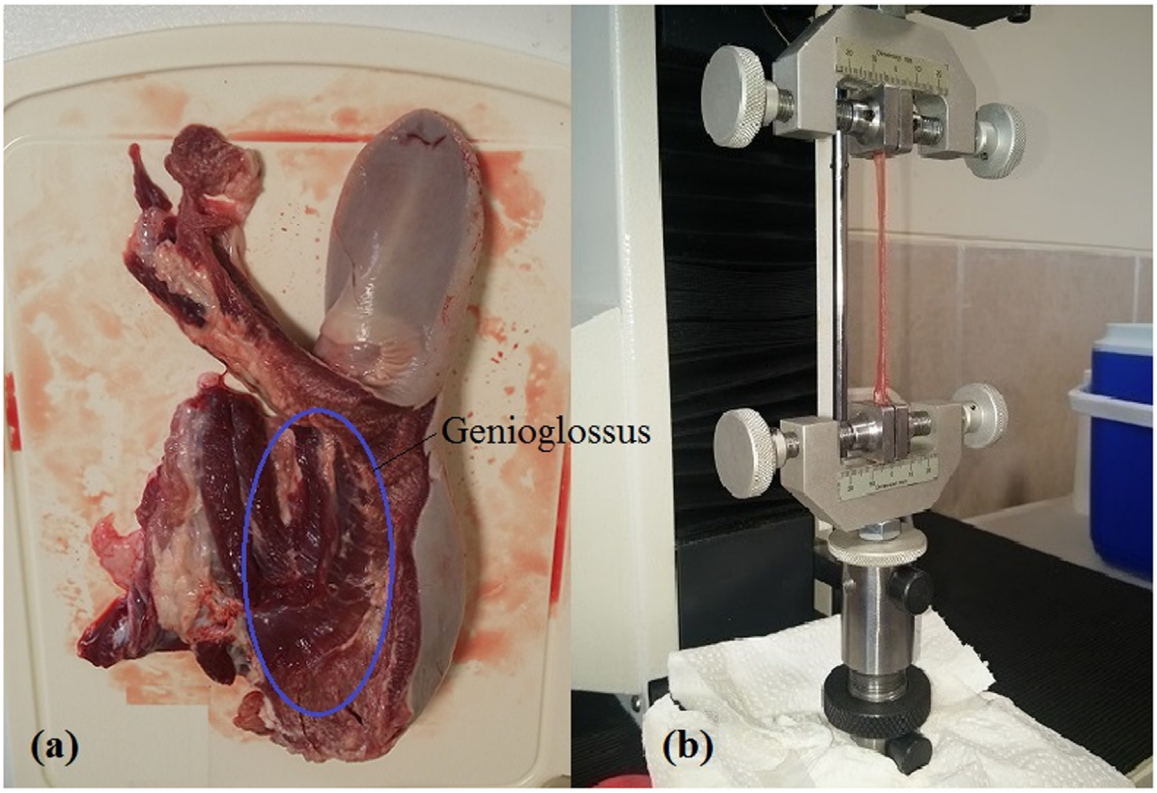

Fig. 4. Bovine tongue (a) and a sample of bovine tongue muscle under uniaxial tension test (b).

Table 1
Geometrical information of the samples dissected from the bovine genioglossus muscle.

Orientation to the muscle fibers	Number of samples (–)	Average length[a] ± std (mm)	Average width ± std (mm)	Average height ± std (mm)
$\phi = 0^{\circ}$	6	49.0 ± 2.7	7.1 ± 0.2	6.5 ± 0.3
$\phi = 45^{\circ}$	5	45.1 ± 3.1	6.6 ± 0.3	6.3 ± 0.2
$\phi = 90^{\circ}$	5	42.3 ± 1.9	6.0 ± 0.3	5.8 ± 0.4

[a] Length means the distance between the grips before starting a test, it does not include the gripped parts of the samples.

for those values of θ, CFs do not undergo any stretch over the reported ranges of stretch in Fig. 5. Theoretically and physically, of course they can be recruited but beyond the reported ranges of stretch. Moreover, c_3 and c_4 vary as θ increases since the CFs become a more contributor to the overall response when the muscle is loaded perpendicular to the MFs direction.

Using these estimated material parameters, the accuracy of the proposed model in Eqs. (7a)–(7c) has been examined at $\phi = 45^{\circ}$. In this case, the nominal stress-stretch relationship is plotted in Fig. 6 together with the standard deviation curves. The proposed model has been implemented in the ABAQUS explicit solver. Nominal stresses for $\theta = 60^{\circ}$, 63°, 65°, and 70° at the most central point of the sample are plotted in Fig. 6. As can be seen from this figure, the proposed passive muscle model with the tuned material parameters for $\theta = 63^{\circ}$ accurately predicts the behavior of the genioglossus muscle. So, it seems that the mean angle between CFs and MFs in the reference configuration might be very close to $\theta = 63^{\circ}$ for the genioglossus tissue.

In order to provide a better understanding of the tensile behavior of muscles predicted by the proposed model, the distribution of the nominal stress P_{11} in each loading direction is shown in Fig. 7. To do this, using the estimated material parameters for the case of $\theta = 63^{\circ}$, 3

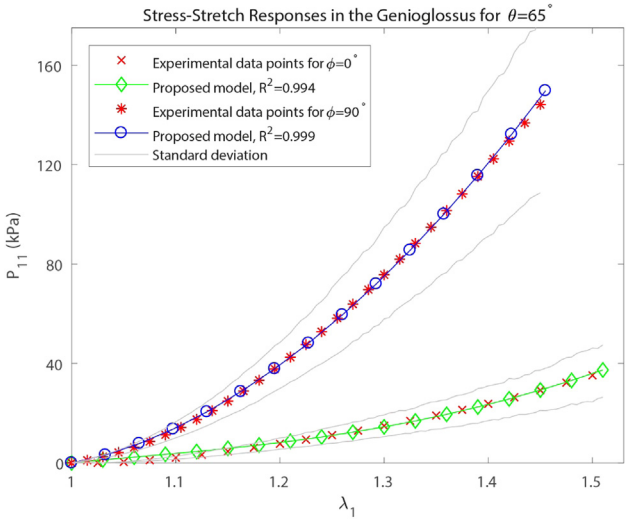

Fig. 5. Stress-stretch responses of the bovine genioglossus muscle tissue to the uniaxial tension tests in different loading angles with respect to the MF direction. Also, the best approximation of the proposed model is plotted.

Table 2
Material parameters of the bovine genioglossus muscle tissue estimated for the proposed model.

	c_1 (kPa)	c_2 (kPa)	c_3 (kPa)	c_4 (–)	k (kPa)	R^2 for $\phi = 0^{\circ}$	R^2 for $\phi = 90^{\circ}$
$\theta = 60^{\circ}$	9.668	7.369	373.012	2.379	1E7	0.992	0.996
$\theta = 63^{\circ}$	10.566	7.034	328.219	2.419		0.994	0.999
$\theta = 65^{\circ}$	10.566	7.034	313.181	2.462		0.994	0.999
$\theta = 70^{\circ}$	10.566	7.034	278.269	2.534		0.994	0.999

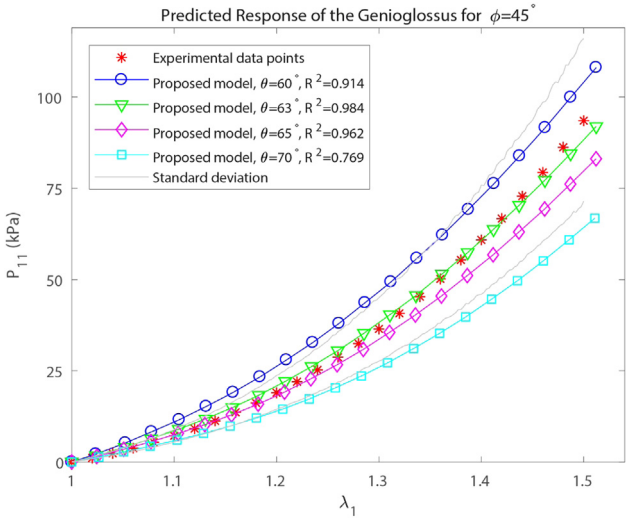

Fig. 6. Comparison of the accuracy of the stress-stretch prediction of the proposed model for the bovine genioglossus muscle tissue in loading at different angles θ.

samples with the same geometrical dimensions 7 mm × 7 mm × 49 mm and the same mesh of the 8-node brick elements underwent a 40% increase in the total length. To apply the boundary conditions, the bottom surface of samples with the normal vector x was pinned and the top surface was subjected to 40% of an increase in length along the x-direction. Moreover, the top surface was fixed in the directions of y and z (Gasser et al., 2006). Fig. 7(b) shows that even in the presence of shear deformations caused by the non-symmetrical distribution of the CFs along the loading direction, the length to width ratio of 7 is sufficient to eliminate the gripping effects and provide a uniform stress distribution in the central part.

Moreover, for the case of $\phi = 90^{\circ}$ in Fig. 7, the transversal stretch ratios λ_y and λ_z are not equivalent which is in agreement with some experimental findings (Takaza et al., 2013; Mohammadkhah et al., 2016). To be more specific, when a sample is loaded in a direction perpendicular to the direction of the muscle fibers, in the transverse plane there will be a higher amount of shortening along the muscle fibers. The authors guess that there are two contributors to this behavior. First, in such condition, the stretched collagen fibers in the plane xz have a compressive component of stress along the muscle fibers. Consequently, the tissue is forced into a biased shortening in that direction. Second, it seemed that the existence of the cross-bridges is something that allows the actin and myosin filaments to have more spaces for shortening even in the passive state. For instance, Fig. 8 shows the initial and deformed shape of the cross-section in the middle section of samples shown in Fig. 7. As depicted in Fig. 8 for the case of $\phi = 90^{\circ}$, the sample underwent a higher amount of shortening in the z-direction which is parallel to the muscle fibers.

4. Model evaluation on literature data

To provide a broader evaluation of our CL, we propose to confront it with experimental data describing the elastic responses of the pig longissimus dorsi muscle tissue (Takaza et al., 2013; Gindre et al., 2013) and the chicken pectoralis muscle (Mohammadkhah et al., 2016).

4.1. Pig longissimus dorsi muscle

The experimental stress-stretch responses of the pig longissimus dorsi muscle were measured at $\phi = 0^{\circ}$, 30°, 45°, 60° and 90° by Takaza et al. (2013). Results show that not only the tissue becomes stronger by increasing the loading angle ϕ but also the curvature of the stress-stretch curve changes. So, it is difficult to find a CL which can smoothly describe this curvature variation with a few number of material parameters. These experimental measurements suggest that the CFs have more contribution to the resultant response when the tissue is loaded at $\phi = 90^{\circ}$ than at $\phi = 0^{\circ}$. So, the angle θ must be greater than 45°. Similar to the method used for the bovine genioglossus muscle tissue, c_{1-4} have been determined for different values of θ. In this case, the Cauchy stress tensor $\boldsymbol{\sigma} = J^{-1}\mathbf{F}\mathbf{S}\mathbf{F}^{T}$ which has been used by Takaza to report the behavior of the longissimus dorsi muscle can be computed from Eqs. (8a)–(8d) and (9). Then, c_{1-4} have been estimated by fitting the Cauchy stress-stretch relationship to the experimental measurements at $\phi = 0^{\circ}$ and 90° according to the procedure proposed in Fig. 3. The estimated values of the parameters c_{1-4} for $\theta = 59^{\circ}$, 63°, and 65° are given in Table 3. Fig. 9 shows the range of the approximated Cauchy stress in the proposed model for these values of θ.

As shown on Fig. 9, the proposed CL with the reported parameters c_{1-4} has been accurately adapted to fit the experimental data. For $\phi = 0^{\circ}$, there is a slight slope change around $\lambda_1 = 1.24$ in the corresponding gray band, which indicates the immediate recruitment of the CFs and their contribution to the resultant stress at $\theta = 59^{\circ}$. Also, similar to the explanations provided to interpret the estimated parameters of Table 2, the parameters c_1 and c_2 approximately remained constant for the cases of $\theta = 63^{\circ}$ and $\theta = 65^{\circ}$ in Table 3 which indicates that over the ranges of stretch used to estimate the material parameters, there would not be any recruitment in the CFs.

Using the estimated material parameters in Table 3, the stress-stretch behavior of the longissimus dorsi muscle has been predicted at $\phi = 30^{\circ}$, 45°, and 60° by implementing the proposed model in Eqs. (7a)–(7c) in the ABAQUS explicit solver. Then, the Cauchy stress at the most central point of the sample is plotted in Fig. 10. In this figure, the range of the predicted stress is depicted inside the gray bands for this specific range $59^{\circ} \leq \theta \leq 65^{\circ}$. Also, coefficient R^2 indicates the goodness of the model prediction with respect to the middle curve of each gray band.

Predicted response for $\phi = 60^{\circ}$ begins with a steep slope which is due to the ability of the proposed model to provide a curvature variation for the tissue response. In this case, although the model prediction does not seem to be acceptable for the small values of the stretch, it will be improved if the CL is replaced with another SEF for the CFs contribution, in which the CFs resistance is more smoothly. Providing such a SEF needs including some extra material parameters in the CL. Also, from the plotted bands of Fig. 10, it is deduced that the mean angle θ in the longissimus dorsi muscle might be in the range of $59^{\circ} \leq \theta \leq 65^{\circ}$ in the reference configuration.

4.2. Chicken pectoralis muscle

To complete the evaluation of our model, we use the elastic stress-stretch data of the chicken pectoralis muscle at $\phi = 0^{\circ}$, 45°, and 90° (Mohammadkhah et al., 2016). The reported results show that the MF direction is the weakest direction in terms of mechanical resistance and the direction along 45° with respect to the MF alignment is the stiffest direction. As a result, according to the proposed passive muscle model, obviously, the CFs have a higher contribution to the overall stress for $\phi = 90^{\circ}$ than for $\phi = 0^{\circ}$. Therefore, the angle θ must be greater than 45°. With the same policy as described above, material parameters c_{1-4} have been estimated for different values of θ by fitting the Cauchy stress-stretch relationship to the experimental measurements at $\phi = 0^{\circ}$ and 90°. The estimated values of the parameters c_{1-4} for $\theta = 51^{\circ}$, 53°, and 55° are given in Table 4. For instance, in the case of $\theta = 53^{\circ}$, Fig. 11 shows the approximated Cauchy stress-stretch relationship in the directions parallel and perpendicular to the MF direction.

For the chicken pectoralis muscle in which the stiffness of the tissue in the directions of $\phi = 0^{\circ}$ and 90° are much closer to each other, there are two possible deductions. First, the distribution of the CFs is similar to the previous two cases but they must be weaker. Second, their

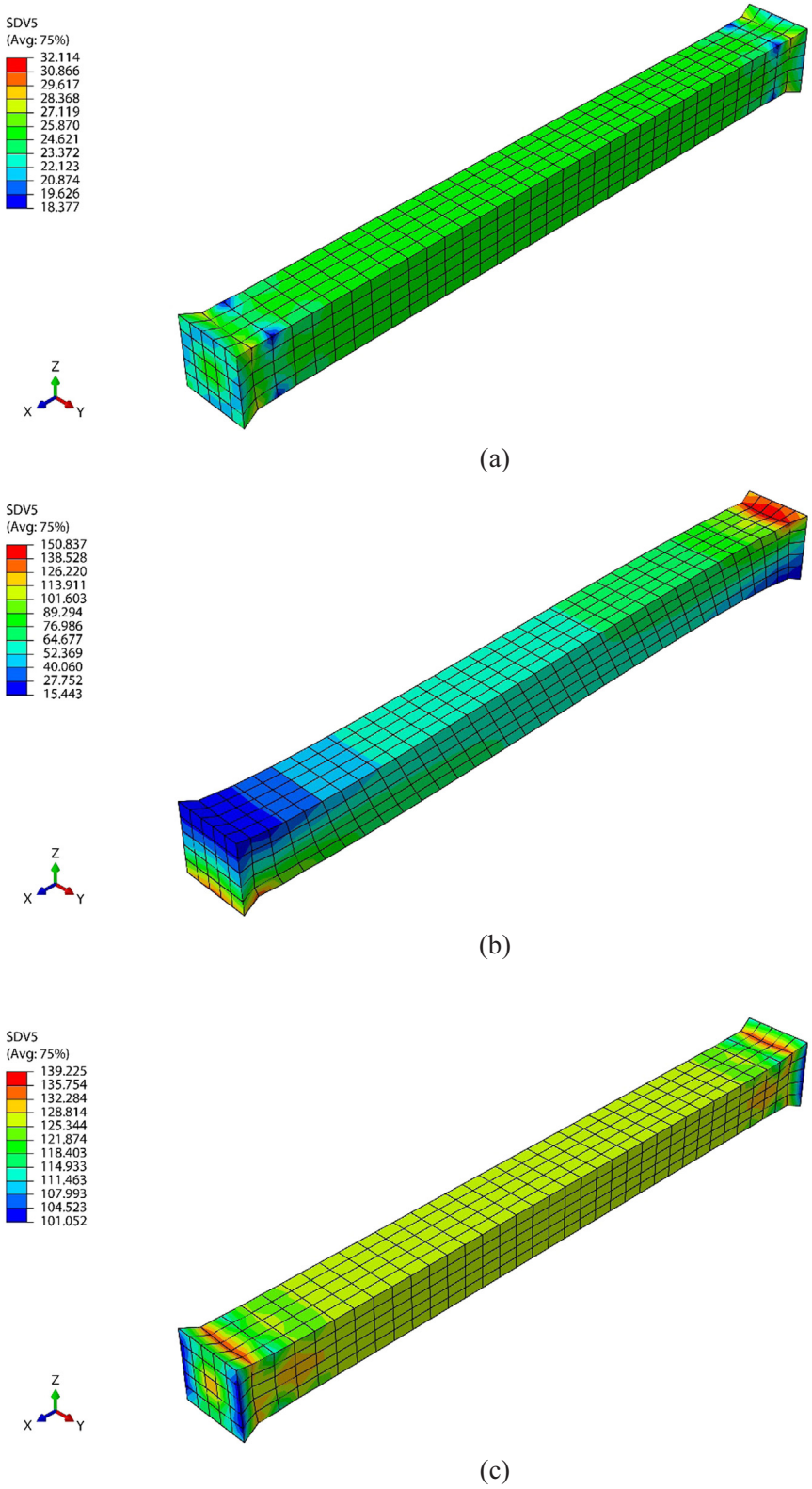

Fig. 7. Distribution of the nominal stress P_{11} after applying 40% of stretch to the total length in the genioglossus muscle for $\theta = 63^{\circ}$. (a) is for $\phi = 0^{\circ}$ and MFs are along the x-direction, in (b) the direction of MFs makes angle $\phi = 45^{\circ}$ with the x-direction in the plane xz, and in (c) MFs are along the z-direction which means $\phi = 90^{\circ}$.

distribution is less aligned to the directions perpendicular to the MFs, it means that θ might have a smaller value. On the other hand, Since chicken pectoralis is stiffer at $\phi = 45^{\circ}$, there must be a family of fibers very close to this direction in order to provide such stiffness. Therefore, the second explanation is anticipated to be the case for the chicken pectoralis muscle.

Finally, using these estimated material parameters, the accuracy of the proposed model has been examined at $\phi = 45^{\circ}$. In this case, the approximated Cauchy stress-stretch relationship is plotted in Fig. 12. The FEA results for $\theta = 51^{\circ}$, 53°, and 55° at the most central point of the

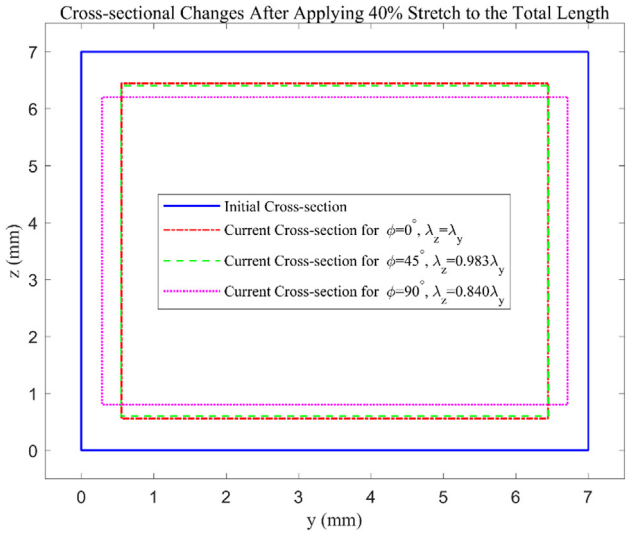

Fig. 8. Changes in the middle cross-section after applying 40% increase to the total length (x-direction) in the genioglossus muscle. In the case of $\phi = 0^{\circ}$, there is a symmetric deformation in the transversal directions y and z. In the case of $\phi = 45^{\circ}$ in which the MFs are in the plane xz, the amount of shear deformation is a parameter that affects the values of the transversal stretches. Also, for $\phi = 90^{\circ}$, the MFs are along the z-direction.

Table 3
Material parameters of the pig longissimus dorsi muscle tissue estimated for the proposed model.

	c_1 (kPa)	c_2 (kPa)	c_3 (kPa)	c_4 (–)	k (kPa)	R^2 for $\phi = 0^{\circ}$	R^2 for $\phi = 90^{\circ}$
$\theta = 59^{\circ}$	89.451	12.194	220.296	1.511	1E7	0.998	0.977
$\theta = 63^{\circ}$	98.736	11.073	251.194	1.637		0.999	0.986
$\theta = 65^{\circ}$	98.750	11.067	216.285	1.630		0.999	0.993

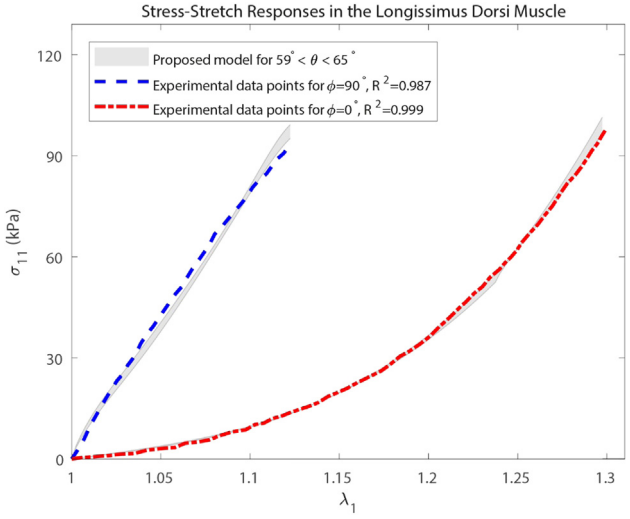

Fig. 9. Stress-stretch responses of the pig longissimus dorsi muscle tissue to the uniaxial tension tests in different loading angles with respect to the fiber direction. Also, the ranges of the best approximations of the proposed model for $\phi = 0^{\circ}$ and 90° are depicted as gray bands.

sample are plotted in this figure. It can obviously be seen from Fig. 12 that the proposed passive muscle model with the tuned material parameters for $\theta = 51^{\circ}$ accurately approximates the behavior of the chicken pectoralis muscle. So, it seems that the angle θ in the reference configuration might be around $\theta = 51^{\circ}$ for this muscle.

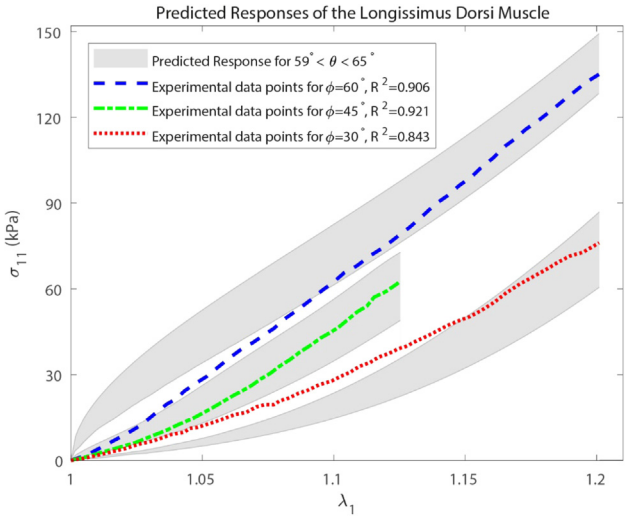

Fig. 10. Comparison of the accuracy of the stress-stretch prediction of the proposed CL for the pig longissimus dorsi muscle tissue in loading at different angles θ.

Table 4
Material parameters of the chicken pectoralis muscle tissue estimated for the proposed model.

	c_1 (kPa)	c_2 (kPa)	c_3 (kPa)	c_4 (–)	k (kPa)	R^2 for $\phi = 0^{\circ}$	R^2 for $\phi = 90^{\circ}$
$\theta = 51^{\circ}$	84.344	9.642	460.859	2.007	1E7	0.999	0.972
$\theta = 53^{\circ}$	121.045	13.489	219.279	1.936		0.999	0.993
$\theta = 55^{\circ}$	137.198	14.877	197.613	2.016		0.998	0.992

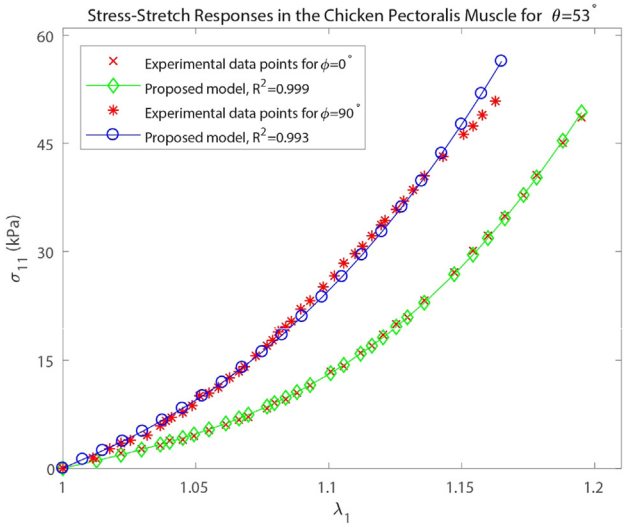

Fig. 11. Stress-stretch responses of the chicken pectoralis muscle tissue to the uniaxial tension tests in different loading angles with respect to the MF direction. Also, the best approximation of the proposed model is plotted.

Besides, there is another approach to model this behavior by defining different Young moduli along each direction (Latorre et al., 2018), but it cannot capture the anisotropy of the tissue. It is remarkable that without any distinction between CFs and MFs in the constitutive law, it is impossible to include the anisotropy and predict such a complex stress-stretch behavior.

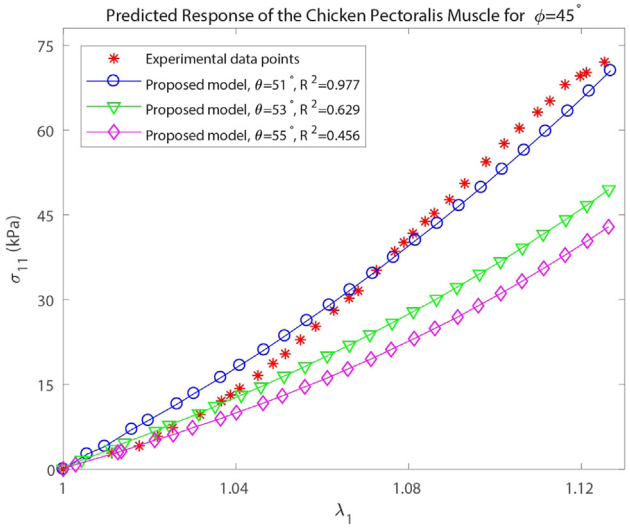

Fig. 12. Comparison of the accuracy of the stress-stretch prediction of the proposed CL for the chicken pectoralis muscle tissue in loading at different angles θ.

5. Discussions

The passive mechanical modeling of muscle tissue is very important in various applications of biomechanical studies. However, most of the proposed passive muscle models in the literature cannot rigorously explain all of the observed stress-stretch behaviors in muscle tissue, especially in tissue that amazingly shows less resistance to the applied load along the fiber alignment. In such muscle models that do not distinguish the MFs and the CFs, approximating such an amazing material behavior might need a negative contribution for the anisotropic part of the stress tensor, which violates the convexity condition of the CL. This paper has proposed a new muscle architecture to overcome these drawbacks by taking into consideration the 3-D distribution of the CFs in the muscle tissue. The model is based on the separation of the CFs and their directions from the MFs in some muscles which first was presented by Purslow (1989). Therefore, in such model, the reinforced direction of muscle tissue is not necessarily parallel to the direction of the MFs and it is dependent on the angle θ between CFs and MFs.

With the aid of an inverse finite element method, an iteration based procedure was proposed for material parameters estimation of muscle tissue under uniaxial tensile tests. Also, it was shown that it is possible to predict the angle θ between CFs and MFs without any dedicated experimental measurement.

The mechanical properties of the bovine tongue tissue were studied by dissecting some samples from the genioglossus muscle tissue and by measuring its response under uniaxial tensile tests. Among the various muscle groups of the tongue, the genioglossus was chosen because of its ability to provide acceptable macroscopic samples in any direction with respect to the MFs. Samples were stretched in different directions to determine the fiber oriented nature of the genioglossus tissue. To demonstrate the relevance and the adequacy of the proposed passive muscle model, it was appraised in the stress-stretch response prediction of the bovine genioglossus muscle tissue, the pig longissimus dorsi muscle and the chicken pectoralis muscle. A good agreement between FEA results and experimental data points in different angles validates the ability of the proposed muscle model in fully taking into account the nonlinear and orientation dependent nature of muscle tissue.

According to the proposed model, without any dedicated experimental measurement for the angle θ, to completely determine the 3-D behavior of muscle tissue, it is required to perform uniaxial tensile tests at least in three different directions. Only for $\theta = 0^{\circ}$, the elastic properties can be determined with two tensile tests. In general, there is no restriction for loading directions, but if tests were performed at $\phi = 0^{\circ}$, 90°, and another arbitrary angle, it would result in less computational costs.

Besides, although the proposed muscle model of this study is based on a simplified distribution of the CFs in muscles, it is the first one that not only can explain the 3-D passive stress response of skeletal muscles but also its transversal stretches approximation is in agreement with some experimental evidence. For instance, when a sample of the longissimus dorsi muscle of pigs with the loading angle $\phi = 90^{\circ}$ is extended to $\lambda_x = 1.15$ (similar to Fig. 7c), our model prediction for the stretch ratios in the transverse plane yz is $\lambda_z = 0.881\lambda_y$ while its experimental value reported as $\lambda_z = 0.938\lambda_y$ (Takaza et al., 2013). For the chicken pectoralis muscle, when the tissue is extended to $\lambda_x = 1.2$, the model approximation and experimental measurement are $\lambda_z = 0.860\lambda_y$ and $\lambda_z = 0.887\lambda_y$, respectively (Mohammadkhah et al., 2016). Regardless of the differences between the experimental measurement and model prediction, the amount of the shortening in the MFs direction approximated by the proposed model always remains higher than the same property in the direction perpendicular to it ($\lambda_z < \lambda_y$). To provide a more accurate approximation for λ_z and λ_y, the model must be improved to consider the orientation dependent behavior of muscles in compression which seems to be necessary for modeling the 3-D responses of muscle tissue even in tensile loading. The sliding ability of the actin and myosin filaments in the passive behavior indicates that a muscle tissue is more likely to be shortened along the MF direction than others when the tissue is stretched non-parallel to the MF direction. So, considering the anisotropic nature of muscle tissue in compressive loading will anticipate the improvement of muscle models accuracy.

Acknowledgments

This work has been supported by Center for International Scientific Studies and Collaboration (CISSC) and French Embassy in Tehran in the framework of the project Hubert Curien Gundishapur BIOSTOC.

Conflicts of interest

The authors declare that they have no conflict of interest.

Appendix A

To show that the final values of the material parameters are independent of a first guess, the identification process has been performed two times for the genioglossus muscle. For the first case, the material parameters with the initial values (a_i) have been provided by the above-described procedure in Fig. 3. In the second case, the initial values (b_i) have been chosen by some random values in the range of $0<b_i\leq 2a_i$. Table A1 shows the

Table A1
Initial values of sets a_i and b_i which have been used to study their effects on the convergence for the case of $\theta = 60^{\circ}$.

Initial value	c_1 (kPa)	c_2 (kPa)	c_3 (kPa)	c_4 (–)
a_i	10.190	6.942	384.739	2.481
b_i	19.192	7.084	182.382	2.925

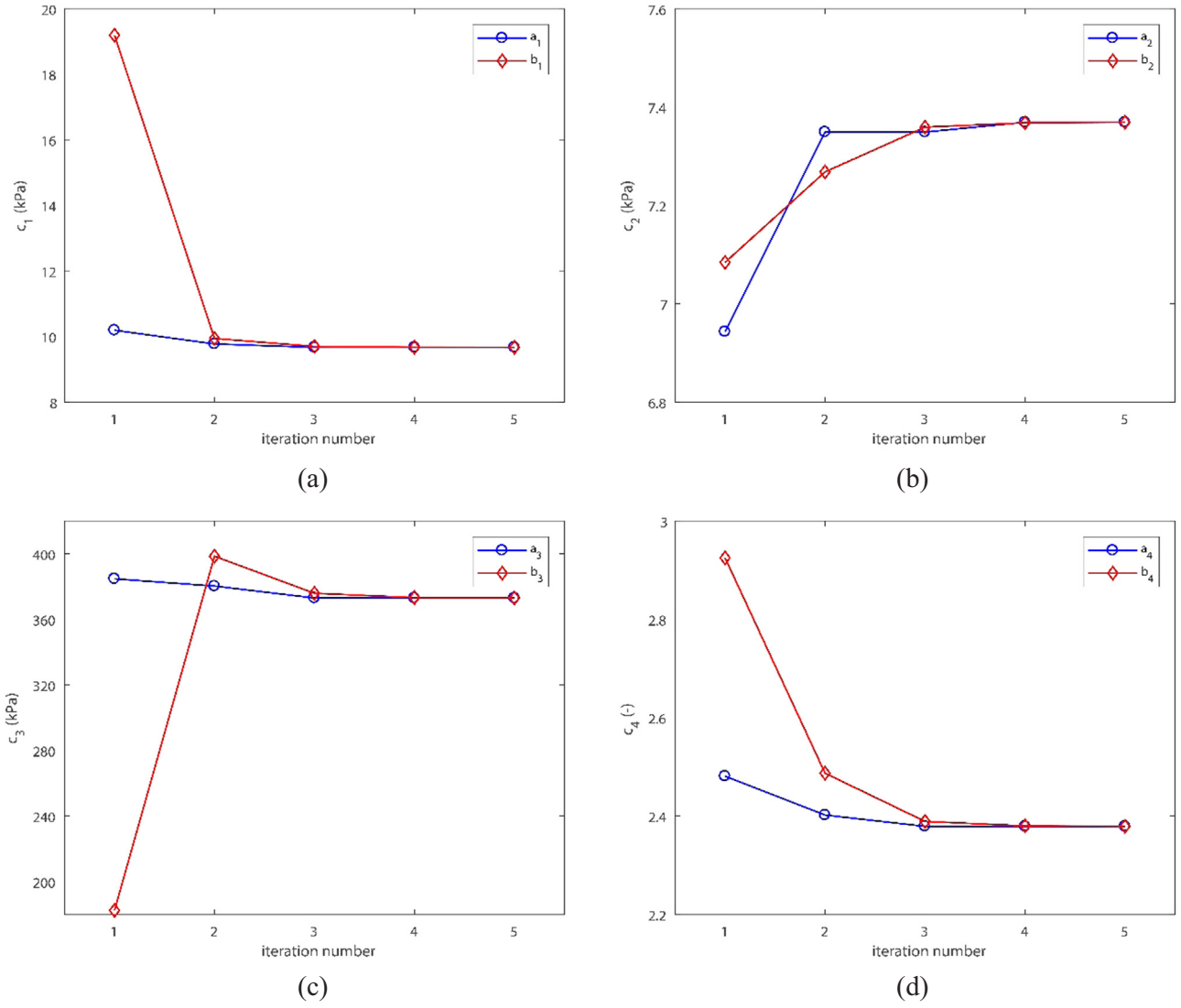

Fig. A1. Convergence study of the material parameters for the case of $\theta = 60^{\circ}$ using two different sets of initial values, graphs (a)–(d) show changes in c_1–c_4 in each iteration, respectively.

initial values chosen for both cases. Also, Fig. A1 shows the convergence history of each material parameters through the optimization process. It is obvious that in both scenarios, the material parameters have been converged to the same values which indicate that their final values are independent of the initial guess.

References

Blemker, S.S., Pinsky, P.M., Delp, S.L., 2005. A 3D model of muscle reveals the causes of nonuniform strains in the biceps brachii. J. Biomech. 38 (4), 657–665.

Böl, M., Kruse, R., Ehret, A.E., Leichsenring, K., Siebert, T., 2012. Compressive properties of passive skeletal muscle—the impact of precise sample geometry on parameter identification in inverse finite element analysis. J. Biomech. 45 (15), 2673–2679.

Böl, M., Ehret, A.E., Leichsenring, K., Weichert, C., Kruse, R., 2014. On the anisotropy of skeletal muscle tissue under compression. Acta Biomater. 10 (7), 3225–3234.

Böl, M., Leichsenring, K., Ernst, M., Ehret, A.E., 2016. Long-term mechanical behaviour of skeletal muscle tissue in semi-confined compression experiments. J. Mech. Behav. Biomed. Mater. 63, 115–124.

Buchaillard, S., Perrier, P., Payan, Y., 2009. A biomechanical model of cardinal vowel production: muscle activations and the impact of gravity on tongue positioning. J. Acoust. Soc. Am. 126 (4), 2033–2051.

Calvo, B., Ramírez, A., Alonso, A., Grasa, J., Soteras, F., Osta, R., Muñoz, M.J., 2010. Passive nonlinear elastic behaviour of skeletal muscle: experimental results and model formulation. J. Biomech. 43 (2), 318–325.

Chagnon, G., Rebouah, M., Favier, D., 2015. Hyperelastic energy densities for soft biological tissues: a review. J. Elast. 120 (2), 129–160.

Dang, J., Honda, K., 2002. Estimation of vocal tract shapes from speech sounds with a physiological articulatory model. J. Phon. 30 (3), 511–532.

Flory, P.J., 1961. Thermodynamic relations for high elastic materials. Trans. Faraday Soc. 57, 829–838.

Fujita, S., Dang, J., Suzuki, N., Honda, K., 2007. A computational tongue model and its clinical application. Oral Sci. Int. 4 (2), 97–109.

Gasser, T.C., Ogden, R.W., Holzapfel, G.A., 2006. Hyperelastic modelling of arterial layers with distributed collagen fibre orientations. J. R. Soc. Interface 3 (6), 15–35.

Gérard, J.M., Ohayon, J., Luboz, V., Perrier, P., Payan, Y., 2005. Non-linear elastic properties of the lingual and facial tissues assessed by indentation technique: application to the biomechanics of speech production. Med. Eng. Phys. 27 (10), 884–892.

Gérard, J.M., Perrier, P., Payan, Y., 2006. 3D biomechanical tongue modeling to study speech production. In: Magnenat-Thalmann, N., Ratib, O., Choi, H.F. (Eds.), Speech Production: Models, Phonetic Processes, and Techniques. Psychology Press, New York, pp. 85–102.

Gilbert, R.J., Wedeen, V.J., Magnusson, L.H., Benner, T., Wang, R., Dai, G., Roche, K.K., 2006. Three-dimensional myoarchitecture of the bovine tongue demonstrated by diffusion spectrum magnetic resonance imaging with tractography. Anat. Rec. Part A: Discov. Mol. Cell. Evolut. Biol. 288 (11), 1173–1182.

Gindre, J., Takaza, M., Moerman, K.M., Simms, C.K., 2013. A structural model of passive skeletal muscle shows two reinforcement processes in resisting deformation. J. Mech. Behav. Biomed. Mater. 22, 84–94.

Goldberg, D.E., 2006. Genetic Algorithms. Pearson Education, India.

Gras, L.L., Mitton, D., Viot, P., Laporte, S., 2012. Hyper-elastic properties of the human sternocleidomastoideus muscle in tension. J. Mech. Behav. Biomed. Mater. 15,

131–140.
Grasa, J., Sierra, M., Lauzeral, N., Munoz, M.J., Miana-Mena, F.J., Calvo, B., 2016. Active behavior of abdominal wall muscles: experimental results and numerical model formulation. J. Mech. Behav. Biomed. Mater. 61, 444–454.
Hernández, B., Pena, E., Pascual, G., Rodriguez, M., Calvo, B., Doblaré, M., Bellón, J.M., 2011. Mechanical and histological characterization of the abdominal muscle. A previous step to modelling hernia surgery. J. Mech. Behav. Biomed. Mater. 4 (3), 392–404.
Hernández-Gascón, B., Peña, E., Pascual, G., Bellón, J.M., Calvo, B., 2014. Can numerical modelling help surgeons in abdominal hernia surgery? In: Giamberardino, P.D., Iacoviello, D., Jorge, R.N., Tavares, J.M.R.S. (Eds.), Computational Modeling of Objects Presented in Images. Springer, Cham, pp. 167–185.
Holzapfel, G.A., 2000. *Nonlinear Solid Mechanics*. 24 Wiley, Chichester.
Humphrey, J.D., Yin, F.C.P., 1987. On constitutive relations and finite deformations of passive cardiac tissue: I. A pseudostrain-energy function. J. Biomech. Eng. 109 (4), 298–304.
Latorre, M., Mohammadkhah, M., Simms, C.K., Montans, F.J., 2018. A continuum model for tension-compression asymmetry in skeletal muscle. *Journal of the mechanical behavior of biomedical materials* 77, 456–460.
Martins, J.A.C., Pires, E.B., Salvado, R., Dinis, P.B., 1998. A numerical model of passive and active behavior of skeletal muscles. Comput. Methods Appl. Mech. Eng. 151 (3–4), 419–433.
Mohammadkhah, M., Murphy, P., Simms, C.K., 2016. The in vitro passive elastic response of chicken pectoralis muscle to applied tensile and compressive deformation. J. Mech. Behav. Biomed. Mater. 62, 468–480.
Morrow, D.A., Donahue, T.L.H., Odegard, G.M., Kaufman, K.R., 2010. Transversely isotropic tensile material properties of skeletal muscle tissue. J. Mech. Behav. Biomed. Mater. 3 (1), 124–129.
Nie, X., Cheng, J.I., Chen, W.W., Weerasooriya, T., 2011. Dynamic tensile response of porcine muscle. J. Appl. Mech. 78 (2), 021009.
Parente, M.P.L., Jorge, R.N., Mascarenhas, T., Fernandes, A.A., Martins, J.A.C., 2009. The influence of the material properties on the biomechanical behavior of the pelvic floor muscles during vaginal delivery. J. Biomech. 42 (9), 1301–1306.
Pioletti, D.P., Rakotomanana, L.R., Benvenuti, J.F., Leyvraz, P.F., 1998. Viscoelastic constitutive law in large deformations: application to human knee ligaments and tendons. J. Biomech. 31 (8), 753–757.
Purslow, P.P., 1989. Strain-induced reorientation of an intramuscular connective tissue network: implications for passive muscle elasticity. J. Biomech. 22 (1), 21–31.
Purslow, P.P., 2010. Muscle fascia and force transmission. J. Bodyw. Mov. Ther. 14 (4), 411–417.
Rohan, P.Y., Lobos, C., Nazari, M.A., Perrier, P., Payan, Y., 2017. Finite element models of the human tongue: a mixed-element mesh approach. Comput. Methods Biomech. Biomed. Eng.: Imaging Vis. 5 (6), 390–400.
Shall, M.S., 2012. Tongue biomechanics and motor control. In: McLoon, L.K., Andrade, F. (Eds.), Craniofacial Muscles. Springer, New York, pp. 229–240.
Schröder, J., Neff, P., 2003. Invariant formulation of hyperelastic transverse isotropy based on polyconvex free energy functions. Int. J. Solids Struct. 40 (2), 401–445.
Song, B., Chen, W., Ge, Y., Weerasooriya, T., 2007. Dynamic and quasi-static compressive response of porcine muscle. J. Biomech. 40 (13), 2999–3005.
Spencer, A.J.M. (Ed.), 1984. Continuum Theory of the Mechanics of Fibre-reinforced Composites 282 Springer, New York.
Stavness, I., Hannam, A.G., Lloyd, J.E., Fels, S., 2006. An integrated dynamic jaw and laryngeal model constructed from ct data. In: Proceedings of the International Symposium on Biomedical Simulation. Springer, Berlin, Heidelberg, pp. 169–177.
Takaza, M., Moerman, K.M., Gindre, J., Lyons, G., Simms, C.K., 2013. The anisotropic mechanical behaviour of passive skeletal muscle tissue subjected to large tensile strain. J. Mech. Behav. Biomed. Mater. 17, 209–220.
Tian, L., Henningsen, J., Salick, M.R., Crone, W.C., Gunderson, M., Dailey, S.H., Chesler, N.C., 2015. Stretch calculated from grip distance accurately approximates mid-specimen stretch in large elastic arteries in uniaxial tensile tests. J. Mech. Behav. Biomed. Mater. 47, 107–113.
Van Loocke, M., Lyons, C.G., Simms, C.K., 2006. A validated model of passive muscle in compression. J. Biomech. 39 (16), 2999–3009.
Van Loocke, M., Lyons, C.G., Simms, C.K., 2008. Viscoelastic properties of passive skeletal muscle in compression: stress-relaxation behaviour and constitutive modelling. J. Biomech. 41 (7), 1555–1566.
Vogt, F., Lloyd, J.E., Buchaillard, S., Perrier, P., Chabanas, M., Payan, Y., Fels, S.S., 2006. Efficient 3D finiteelement modeling of a muscle-activated tongue. In: Proceedings of the International Symposium on Biomedical Simulation. Springer, Berlin, Heidelberg, pp. 19–28.
Wheatley, B.B., Odegard, G.M., Kaufman, K.R., Donahue, T.L.H., 2016. How does tissue preparation affect skeletal muscle transverse isotropy? J. Biomech. 49 (13), 3056–3060.
Wheatley, B.B., Odegard, G.M., Kaufman, K.R., Donahue, T.L.H., 2017. A validated model of passive skeletal muscle to predict force and intramuscular pressure. Biomech. Model. Mechanobiol. 16 (3), 1011–1022.
Yousefi, A.A.K., Nazari, M.A., Perrier, P., Panahi, M.S., Payan, Y., 2018. A visco-hyperelastic constitutive model and its application in bovine tongue tissue. J. Biomech. 71, 190–198.